# Integration of RIS into CloudRT Simulator for Railway Tunnel Scenarios

Aline Habib, Charlotte Langlais, Ammar El Falou, Souleymane Kangoute, Yiran Wang, Marion Berbineau

# Integration of RIS into CloudRT Simulator for Railway Tunnel Scenarios

Aline Habib*, Charlotte Langlais*, Ammar El Falou†, Souleymane Kangoute*, Yiran Wang§, Marion Berbineau¶

* Mathematical and electrical engineering department, CNRS UMR 6285 Lab-STICC, IMT Atlantique, Brest, France
† CEMSE Division, King Abdullah University of Science and Technology (KAUST), Saudi Arabia
§ School of Electronic and Information Engineering, Beijing Jiaotong University, Beijing, China
¶ COSYS-LEOST, Université Gustave Eiffel, Villeneuve d'Ascq, France

Email: aline.habib@imt-atlantique.fr

***Abstract*—Radio communication in tunnels presents significant challenges due to the high likelihood of signal obstruction by elements like tunnel walls, ceilings, train carriages, or blocked trains. Reconfigurable Intelligent Surfaces (RIS) offer a promising and cost-effective solution to mitigate signal-blocking issues by transforming the unpredictable radio environment into a controllable one through managed reflections. This paper extends the CloudRT ray-tracing simulator to accommodate RIS technology and assesses its feasibility for railway tunnel scenarios. RIS is integrated into the CloudRT simulator as a phased antenna array acting as a virtual receiver (Rx)/ transmitter (Tx). The study then explores how various key parameters influence received power and compares two scenarios: one where a masking train obstructs the direct Tx-Rx path, and another where there is no obstruction. The results underscore the potential benefits of deploying RIS in obstructed tunnel environments.**

***Index Terms*—Reconfigurable intelligent surface, ray tracer, obstructed tunnel, received power, railway.**

## I. Introduction

Railway environments require high data rates to meet mission-critical communication needs and serve many passengers [1], [2]. Millimeter-wave (mmWave) bands, ranging from 30 to 300 GHz, are increasingly being explored for railway communication systems due to their potential for high data rates [3]. However, waves in these bands are vulnerable to transmission losses and blockage, limiting the coverage area. Moreover, in confined environments, particularly in tunnels, transmitted signals are likely blocked by numerous obstacles, such as tunnel walls, masking trains, and train carriages [4]. In this context, reconfigurable intelligent surface (RIS) is a promising solution to solve the blocking problem of mmWave in the tunnel. This recent technology extends coverage through additional virtual LOS paths [5]. RIS consists of a surface of low-cost passive reflecting elements. These elements reflect incoming waves as a beam in the desired direction according to a controlled phase shift, making the communication controllable [6]. Recently, many studies have focused on investigating RIS in the railway communications sector. The authors in [2] demonstrated that RIS can enhance railway communication by, i) expanding coverage at a reduced cost, ii) mitigating rapid signal strength variations caused by Doppler shift through real-time phase adjustments, and iii) improving both the spectral efficiency and reliability of the railway network. The authors in [7] studied the feasibility of using RIS to solve the problem of interference in railway communications in the presence of jammers. [8] aimed to find the best location of RIS to reduce the delay spread in high-speed train (HST) communications. The authors verified that deploying RIS on the train side mitigates delay spread and improves spectral efficiency. However, few studies have explored the application of RIS in tunnels. [9] examines the effectiveness of RIS in reducing the blocking probability (BP) in an obstructed rectangular tunnel. The authors showed that deploying a sufficient number of RIS with the appropriate configuration decreases the BP. Moreover, in the previous papers, only theoretical channel models are considered, such as Rayleigh and Rice models, whereas they do not well model mmWave propagation channels in a tunnel [10]. Given the challenges of sounding and measuring mmWave channels in a tunnel, the ray tracer simulator serves as an appropriate tool for accurately modeling realistic geometries and generating reliable channels for this environment. However, RIS is not an integrated device in a ray tracer simulator and the reflection applied in the ray tracer follows the Snell-Descartes law. To extend the ray tracer to include RIS, it is necessary to modify the traditional reflection of the ray tracer to obtain a directional reflection. Different methods have been applied in the literature to achieve directional reflection. In [11], the authors applied a rotation of the normal Snell-Descartes to reflect the wave in the desired direction to integrate RIS functionality into a ray tracer simulator called Wireless Insite. In [12], the authors considered the RIS as steerable interaction points acting first as receivers and then as transmitters. The expression of the electromagnetic field at the receiver was modified to take account of the RIS phase shift. In [13], the RIS was modeled as a virtual phased antenna array, which acts first as an Rx and then as a Tx. This paper therefore integrates RIS into a ray-tracer simulator to explore RIS-assisted mmWave communications in railway tunnels where the Tx-Rx link is obstructed by a masking train. Choosing the high-performance tool CloudRT, the study performs two simulations separately: one for the Tx-RIS channel and the other for the RIS-Rx channel. The

RIS elements are first represented as receive points, then as transmit points. Moreover, to reduce heavy computations in CloudRT, RIS is modeled as an array steering vector, avoiding the need to simulate every link between the Tx (resp. RIS) and each RIS element (resp. Rx). The rest of the paper is structured as follows. Section II presents the CloudRT simulator. Section III describes the modeling of an arched tunnel scene. The system model and the approach used to integrate the RIS into CloudRT are introduced in Section IV. Numerical results are presented in Section V. Finally, Section VI concludes the paper.

## II. CloudRT simulator

The high-performance computing cloud-based ray-tracing simulation platform (CloudRT, http://www.raytracer.cloud) is developed by Beijing Jiaotong University [14]. By effectively reproducing multipath components (MPCs) in radio wave propagation, CloudRT can provide accurate and abundant multi-dimensional MPCs information. It operates in static and dynamic environments, including outdoor and indoor scenarios for frequencies ranging from 450 MHz to 325 GHz.

The environment library, material library, and antenna library of the platform offer a wealth of resources for users, enabling users to streamline the simulation setup. To ensure the simulation runs smoothly, some key input parameters including simulation frequency, snapshot, transmitter information, receiver information, and propagation mechanisms are also required. We define the existence of direct and reflected rays, the number of reflections, scattered and transmission rays, and a JSON file describing the geometric model [15]. The three-dimensional geometric model of the scene can be created using the SketchUp tool [16]. Once the simulation configuration is complete, the project can be uploaded for processing. Subsequently, the RT simulation results can be downloaded with detailed information on the rays, including the ray type, delay for each ray, complex field strengths, path loss, angle of arrival (AoA), angle of departure (AoD), section plane, and intersection points, etc., are obtained [17]. In addition, key channel parameters such as path loss, Power Delay Profile (PDP), root-mean-square delay spread, Rician K-factor, and channel transfer function can be calculated.

The reliability of the CloudRT platform has been thoroughly validated through extensive measurements [18]. High computational speed, high precision, and the modeling of mobile scattering objects make it stand out compared to other ray-tracing simulators [19].

## III. Scene of Tunnel

To accurately model and understand the propagation characteristics of mmWave signals assisted by a RIS in a tunnel, a double-track tunnel was designed, measuring 100 meters in length along the x-axis. This module with a rounded shape offers better structural resistance. The tunnel measures 5 meters in height along the z-axis and 9 meters in width along the y-axis. The tunnel entrance starts at 50 meters along the x-axis. The cross-section is arched, with concrete walls. Classical ray tracing models are invalid for such curved surfaces, as explained in [20], where curved surfaces generate infinite images with the image method, rendering them inapplicable. Additionally, curved surfaces do not conserve reflection angles, making ray tracing unsuitable. To address this issue, a faceting technique proposed by the authors in [20] has been integrated into the 3D modeling software SketchUp [16], allowing curved surfaces to be represented as a series of multiple flat surfaces determined by the arc radius. Fig. 1 illustrates an arched tunnel scene comprising 14 facets, designed using SketchUp.

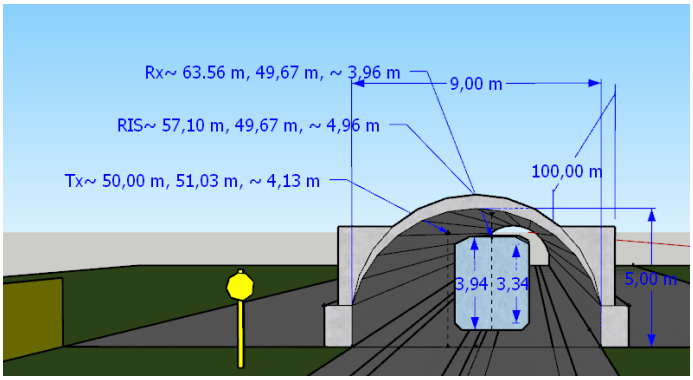


Fig. 1: Arched tunnel entrance

## IV. System model

We investigate a single-input single-output (SISO) mmWave narrowband downlink system assisted by an RIS in a tunnel environment. Fig. 1 illustrates the three-dimensional model of an arched tunnel scenario with a train inside. The Tx transmits signals to a train via a mobile relay (MR) mounted on the train roof to minimize penetration loss through the RIS. The Tx is placed at the tunnel entrance at coordinates (50 m, 51.03 m, 4.13 m), the RIS is deployed on the tunnel ceiling at coordinates (57.10 m, 49.57 m, 3.96 m), and the MR is located at (63.56 m, 49.67 m, 4.96 m) as shown in Fig. 1. Simulation parameters are shown in Table I.

### A. RIS-assisted channel modeling

RIS is considered an additional Rx/Tx when integrating with CloudRT. Consequently, three channels exist. 1) Channel between Tx and RIS, denoted by $\mathbf{H}$, 2) Channel between RIS and Rx, denoted by $\mathbf{G}$, and 3) Direct channel between Tx and Rx, denoted by $\mathrm{H}_d$. This method of integrating RIS into the CloudRT simulator is similar to the approach used to integrate RIS into a stochastic simulator NYUSIM, described in [21]. Three simulations are run at frequency $f$= 30 GHz to determine the corresponding channel coefficients. Fig. 2 shows the rays between Tx-Rx, Tx-RIS, and RIS-Rx resulting from the three ray-tracing simulations in the tunnel scene and the corresponding power delay profile. Two types of rays are presented: direct rays, in red, and reflected rays, in blue, which bounce off objects in the scene before reaching the Rx. Scattered and transmitted rays are not considered, as their impact at mmWave frequencies is minimal [22]. The simulator provides the coordinates of the intersection points

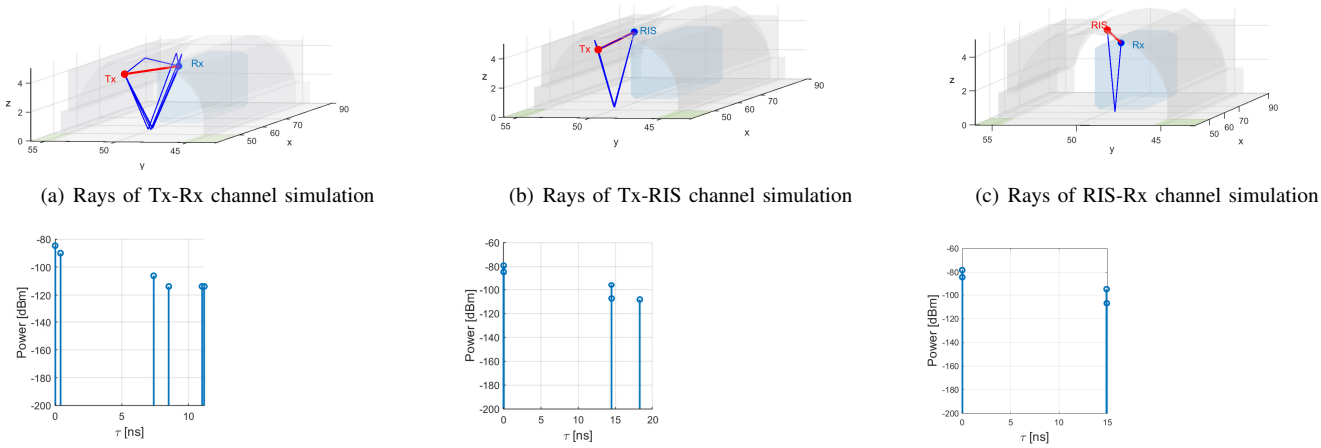


(a) Rays of Tx-Rx channel simulation (b) Rays of Tx-RIS channel simulation (c) Rays of RIS-Rx channel simulation

(d) PDP of Tx-Rx channel (e) PDP of Tx-RIS channel (f) PDP of RIS-Rx channel

Fig. 2: Channel simulations with corresponding power delay profile for RIS-assisted systems in tunnel scene.

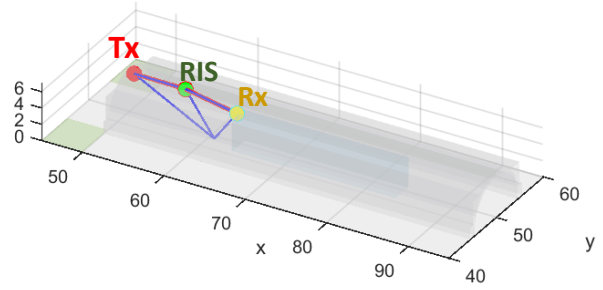


Fig. 3: Combination of Tx-RIS and RIS-Rx channel rays.

where the reflected rays bounce off the scene surfaces. It is clear from this figure that the RIS introduces new multipath components with distinct delays. This suggests that the RIS can be viewed as an artificial multipath source that improves signal strength at the Rx by creating additional propagation paths. We assume that the direct Tx-Rx channel does not exist. Thus, the Rx receives signals only from the RIS. Fig. 3 shows the combination of rays obtained from the simulations, Tx-RIS and RIS-Rx. Each train position is considered a snapshot in CloudRT in moving train scenarios. Using CloudRT, parallel simulations are run for these snapshots, with only the Rx coordinates varying. Generally, the channel impulse response for each snapshot s is defined as

$$h(\tau, s) = \sum_{k=1}^{K_s} \alpha_{k,s} e^{j\phi_{k,s}} \delta(\tau - \tau_{k,s}) \tag{1}$$

where $K_s$ is the number of rays obtained by snapshot s, $\phi_{k,s}$, $\tau_{k,s}$ and $\alpha_{k,s}$ are the phase, the amplitude, and the delay of the $k$-th ray of the snapshot s, respectively. These parameters are obtained by ray tracer simulation.

We consider a narrowband system, where rays are assumed to arrive in the same time cluster, and the train is not in motion. Therefore, CIR is equivalent to

$$h_{NB}(\tau) \approx \sum_{k=1}^{K} \alpha_k e^{j\phi_k} \delta(\tau) \tag{2}$$

where $K$ is the number of rays, $\phi_k$, $\tau_k$ and $\alpha_k$ are the phase, the amplitude, and the delay of the $k$-th ray, respectively.

Considering the RIS as a virtual Rx (resp. Tx), the RIS elements, assumed to be $M$, are first represented as $M$ receive (resp. transmit) points for the Tx-RIS (resp. RIS-Rx) channel. The complex-valued coefficient representing the link between the Tx and the $m$-th RIS element is defined as follows

$$h_m = \sum_{k=1}^{K(m)} \alpha_k(m) e^{j\varphi_k(m)} \tag{3}$$

with $K(m)$ the number of resulting rays in the $m$-th simulation, $\varphi_k(m)$ and $\alpha_k(m)$ the phase and the amplitude of the $k$-th ray in the $m$-th simulation. To determine $\mathbf{H} = (h_1, ..., h_M)$, the total channel coefficients between Tx and RIS, we simulate $M$ links corresponding to $M$ RIS elements. The same method can be applied to find the channel coefficients between RIS and Rx, $\mathbf{G}$, except that now the $m$-th RIS element acts as a Tx, rather than a Rx.

### *B. Simplified method using the array steering vector*

Simulating $M$ links is time-consuming, especially for a large number of RIS elements To mitigate this, we first simulate one link between the Tx and the first RIS element seen as a reference element, then apply the array steering vector to determine $\mathbf{H}$. This simplified method is applied in [23] to generate the MIMO channel matrix coefficient in ray tracer. Similarly, for the channel $\mathbf{G}$, we simulate the link between the first RIS element and the Rx, and then apply the array steering vector at the transmission. Therefore, $\mathbf{H}$ and $\mathbf{G}$ can be defined as follows:

$$\mathbf{H} = \sum_{k_1=1}^{K_1} \alpha_{k_1} e^{j\varphi_{k_1}} \mathbf{a}_{RIS}(\vec{\Theta}^a_{k_1}) \tag{4}$$

$$\mathbf{G} = \sum_{k_2=1}^{K_2} \alpha_{k_2} e^{j\varphi_{k_2}} \mathbf{a}_{RIS}(\vec{\Theta}^d_{k_2}) \tag{5}$$

where $K_1$ and $K_2$ denote the number of rays obtained by the Tx-RIS and RIS-Rx simulations, respectively. $\mathbf{a}_{RIS}(\vec{\Theta}^a_{k_1})$ and $\mathbf{a}_{RIS}(\vec{\Theta}^d_{k_2})$ represent the array steering vectors at the RIS, corresponding to the AoA from Tx to RIS and the AoD from the RIS to the Rx, respectively.

The array steering vector $\mathbf{a}(\vec{\Theta})$ for a uniform rectangular antenna array positioned in the $xoy$ plane, consisting of $M_h$ horizontal antennas and $M_v$ vertical antennas, which performs a directional transmission at an angle $\vec{\Theta} = (\theta, \phi)$, is defined as follows.

$$\mathbf{a}(\vec{\Theta}_k) = \left[1, \cdots, e^{-j2\pi \frac{d}{\lambda}\{(M_h-1)\cos(\theta_k)\cos(\phi_k)+(M_v-1)\sin(\phi_k)\}}\right]^T \tag{6}$$

with $j \triangleq \sqrt{-1}$ the imaginary unit, $\lambda$ the carrier wavelength and $d$ the inter-element spacing distance.
The cascaded channel from the Tx to the Rx via the RIS can be defined as

$$C = \mathbf{G}^H \Phi \mathbf{H} \tag{7}$$

Where $\Phi$ is the diagonal matrix representing the RIS phase shifts, given by:

$$\Phi = \text{diag}(\beta_1 e^{j\phi_1}, ....\beta_m e^{j\phi_m}, ...\beta_M e^{j\phi_M}) \tag{8}$$

with $\beta_m$ and $\phi_m$ represent the amplitude and phase shift of $m$-th RIS element, respectively. We assume there is no reflection loss or gain, so $\beta_m = 1, \forall m$. Therefore, the received power is defined as

$$P_r = 10\log_{10}(|C|^2) \tag{9}$$

Next, we present the simulation results, showing the effectiveness of the RIS-assisted mmWave communication in the tunnel environment.

## V. Simulation Results

TABLE I: Simulation Parameters.

| Parameters | Value |
|---|---|
| Frequency | 30 [GHz] |
| RIS elements separation distance | $\lambda/2$ |
| Transmission power $P_t$ | 0 [dBm] |
| Antennas | Omnidirectional vertical polarisation |
| Rays | Direct+reflection |
| Order of reflection | 2 |
| RIS size for $M = 10000$ elements | $50 \times 50$ cm$^2$ |

### A. Order of reflection

The reflection order is the maximum number of reflections possible for the reflected ray to reach the Rx. A compromise is needed between the accuracy of the simulation obtained by increasing the reflection order and the computing time required for the simulation. To determine the sufficient order of reflection, we plot in Fig.4 the power received by the Rx as a function of the Tx-Rx separation distance for different orders of reflection. As seen in this figure, the power received remains relatively constant from a reflection order equal to 2, so we can assume that a reflection order equal to 2 is enough. As stated in [24], a reflection order of 1 or 2 is adequate for mmWave under LoS conditions.

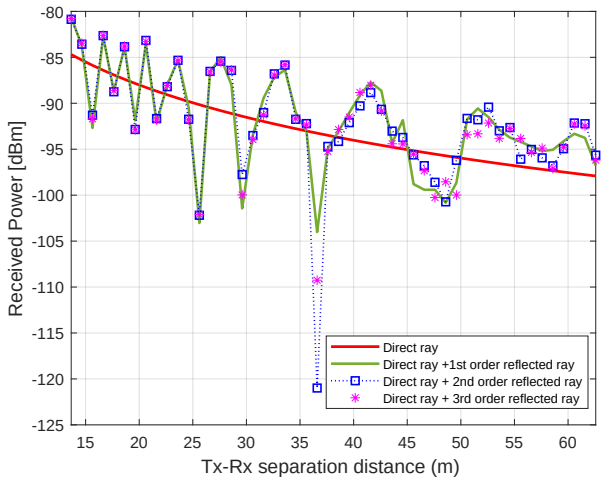


Fig. 4: Power received by the Rx as a function of Tx-Rx separation distance, $d$, for different reflection orders.

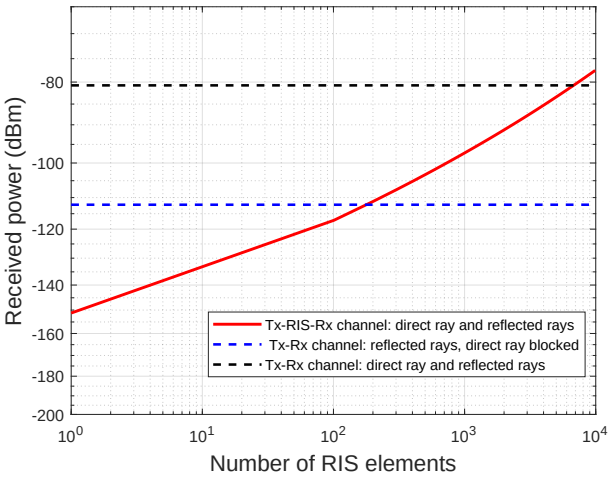


Fig. 5: Received power versus the number of RIS elements for the Tx-Rx link with and w/o masking train and the indirect link via RIS.

### B. RIS-assisted masking train scenario

To investigate RIS empowerment, we plot in Fig. 5 the power received by the Rx in an obstructed tunnel versus the number of RIS elements through the direct Tx-Rx channel, the indirect Tx-RIS-Rx channel[1], and the direct Tx-Rx channel where there is no signal blockage. We modeled a masking train at x = 52 m to represent an obstructed tunnel. The masking train blocks the direct ray between the Tx and the

[1]In simulating the indirect link with the masked train, we assume that the Rx only receives signals from the RIS. Although the reflected rays from the Tx-Rx link exist, we ignore them and focus only on the RIS's contribution to system performance.

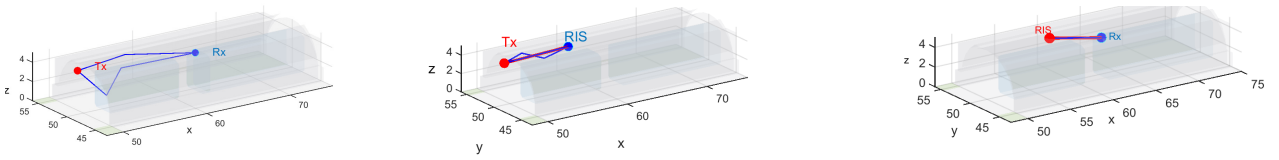


(a) Rays of Tx-Rx channel simulation (b) Rays of Tx-RIS channel simulation (c) Rays of RIS-RX channel simulation

Fig. 6: Channel simulations for RIS-assisted masking train scenario.

Rx, as shown in Fig.6(a). Fig. 6 further illustrates the resulting rays between Tx-RIS and RIS-Rx. The results in Fig. 5 show that the power received via the indirect link through the RIS increases with the number of RIS elements, compensating for the double-path-loss caused by cascaded channels. Moreover, a significant increase in RIS elements allows the indirect link to outperform the Tx-Rx direct link. However, with 100 or fewer RIS elements, the indirect link performs worse than the Tx-Rx direct link when the direct ray is blocked, highlighting the limitations of passive RIS with a small number of elements due to the double-path-loss issue. Therefore, using RIS is crucial when the direct Tx-Rx link is blocked, especially when the number of RIS elements is large.

## VI. Conclusion

In this paper, we investigated the channel model of a RIS-assisted SISO mmWave communication system in a confined arched tunnel scenario using the CloudRT ray-tracing tool. We first integrated RIS into CloudRT as a virtual Rx/Tx phased antenna array to generate realistic channels for this system. The simulation results revealed that i) increasing the number of RIS elements enhances the received power, ii) a reflection order of 2 is sufficient for this system, and iii) RIS is especially critical in obstructed tunnel scenarios where the direct Tx-Rx link is blocked. The multi-RIS-assisted system in a tunnel environment is left as future work. Furthermore, it would be interesting to compare the effectiveness of RIS in other types of tunnels, such as curved tunnels and narrow single-track tunnels, which have a higher likelihood of signal blockage.

## Acknowledgment

This work was funded by the council of the Region Bretagne, under the grant MILLIRIS and the French ANR project mmW4Rail.

## References

[1] A. Habib, A. El Falou, C. Langlais, and M. Berbineau, "Reconfigurable intelligent surface assisted railway communications: A survey," in *Proc. IEEE Vehicular Technology Conference (VTC)*, 2023.

[2] J. Zhang *et al.*, "RIS-aided next-generation high-speed train communications: Challenges, solutions, and future directions," *IEEE Wireless Commun.*, vol. 28, no. 6, pp. 145–151, 2021.

[3] K. Guan *et al.*, "5G channel models for railway use cases at mmWave band and the path towards terahertz," *IEEE Intell. Transp. Syst. Mag.*, vol. 13, no. 3, pp. 146–155, 2021.

[4] H. Liu, J. Liang, K. Chen, and T. Liao, "Wireless channel simulation and measurement of maglev tunnel," in *Information Communication Technologies Conference (ICTC)*, 2022, pp. 25–32.

[5] C. Liu *et al.*, "Coverage probability analysis of RIS-assisted high-speed train communications," in *IEEE Wireless Commun. and Net. Conf. (WCNC)*, 2023.

[6] A. Araghi *et al.*, "Reconfigurable intelligent surface in the sub-6 GHz band: Design, implementation, and real-world demonstration," *IEEE Access*, vol. 10, pp. 2646–2655, 2022.

[7] Z. Ma, Y. Wu, M. Xiao, G. Liu, and Z. Zhang, "Interference suppression for railway wireless communication systems: A reconfigurable intelligent surface approach," *IEEE Trans. Veh. Technol.*, vol. 70, no. 11, pp. 11 593–11 603, 2021.

[8] K. Wang, C.-T. Lam, and B. K. Ng, "How to deploy RIS to minimize delay spread in HST communications: Railroad side, or train side?" in *Int. Conf. Commun. Technol. (ICCT)*, 2022, pp. 793–797.

[9] C. Chen and C. Pan, "Blocking probability in obstructed tunnels with reconfigurable intelligent surface," *IEEE Commun. Lett.*, vol. 26, no. 2, pp. 458–462, 2021.

[10] H. Liu, J. Liang, K. Chen, and T. Liao, "Wireless channel simulation and measurement of maglev tunnel," in *2022 3rd Information Communication Technologies Conference (ICTC)*, 2022, pp. 25–32.

[11] J. Huang, C.-X. Wang, Y. Sun, J. Huang, and F.-C. Zheng, "A novel ray tracing based 6G RIS wireless channel model and RIS deployment studies in indoor scenarios," in *Annual Int. Symp. on Personal, Indoor and Mobile Radio Commun. (PIMRC)*, pp. 884–889.

[12] J. Pyhtilae, J. Kokkoniemi, P. Sangi, N. Vaara, and M. Juntti, "Ray tracing based radio channel modelling applied to RIS," in *WSA & SCC; Int. ITG Workshop Smart Antennas Conf. Syst. Commun. Coding*, 2023.

[13] J. Huang *et al.*, "Ray tracing based 6G RIS-assisted MIMO channel modeling and verification," in *IEEE/CIC Int. Conf. Commun. China (ICCC)*, 2023.

[14] D. He *et al.*, "Physics and AI-based digital twin of multi-spectrum propagation characteristics for communication and sensing in 6G and beyond," *IEEE J. Sel. Areas in Commun.*, vol. 41, no. 11, pp. 3461–3473, 2023.

[15] L. Ma *et al.*, "Characterization for high-speed railway channel enabling smart rail mobility at 22.6 GHz," in *IEEE Wireless Commun. and Net. Conf. (WCNC)*, 2020.

[16] Trimble Inc., "SketchUp," https://www.sketchup.com/fr, n.d., accessed: 2024-10-16.

[17] D. He, B. Ai, K. Guan, L. Wang, Z. Zhong, and T. Kürner, "The design and applications of high-performance ray-tracing simulation platform for 5G and beyond wireless communications: A tutorial," *IEEE Commun. Surv. & Tutorials*, vol. 21, no. 1, pp. 10–27, 2019.

[18] K. Guan *et al.*, "Key technologies for wireless network digital twin towards smart railways," *High-speed Railway*, vol. 2, no. 1, 2024.

[19] L. Wang *et al.*, "An accelerated algorithm for ray tracing simulation based on high-performance computation," in *Int. Symp. on Antennas, Propagation and EM Theory (ISAPE)*, 2016, pp. 512–515.

[20] E. Masson, "Etude de la propagation des ondes électromagnétiques dans les tunnels courbes de section non droite pour des applications métro et ferroviaire," Ph.D. dissertation, Université de Poitiers, 2010.

[21] A. Habib, I. Khaled, A. El Falou, and C. Langlai, "Extended NYUSIM-based mmWave channel model and simulator for RIS-assisted systems," *European Conf. on Net. and Commun. (EUCNC)*, 2023.

[22] F. Fuschini *et al.*, "Analysis of in-room mm-wave propagation: Directional channel measurements and ray tracing simulations," *Journal of Infrared, Millimeter, and Terahertz Waves*, vol. 38, pp. 727–744, 2017.

[23] J. Weng, X. Tu, Z. Lai, S. Salous, and J. Zhang, "Indoor massive MIMO channel modelling using ray-launching simulation," *Int. J. Antennas Propag.*, vol. 2014, no. 1, p. 279380, 2014.

[24] D. Steinmetzer, J. Classen, and M. Hollick, "mmTrace: Modeling millimeter-wave indoor propagation with image-based ray-tracing," in *IEEE Conf. Comput. Commun. Workshop (INFOCOM WKSHPS)*, 2016, pp. 429–434.